Magnetic order and electronic phase diagrams of electron-doped copper oxide materials

G. M. Luke, L. P. Le, B. J. Sternlieb, and Y. J. Uemura
Department of Physics, Columbia University, 538 West 120th Street, New York, New York 10027

J. H. Brewer, R. Kadono,* R. F. Kiefl, S. R. Kreitzman, and T. M. Riseman
Department of Physics, University of British Columbia, Vancouver, Canada V6T 2A3

C. E. Stronach and M. R. Davis
Department of Physics, Virginia State University, Petersburg, Virginia 23803

S. Uchida and H. Takagi
Engineering Research Institute, University of Tokyo Yayoi, Tokyo 113, Japan

Y. Tokura
Department of Physics, University of Tokyo, Hongo, Tokyo 113, Japan

Y. Hidaka and T. Murakami
NTT Opto-Electronics Laboratories, 162 Tokai, Ibaraki 319-11 Japan

J. Gopalakrishnan, A. W. Sleight,† and M. A. Subramanian
E. I. DuPont de Nemours & Co. Experimental Station, Wilmington, Delaware 19880-0262

E. A. Early, J. T. Markert,‡ M. B. Maple, and C. L. Seaman
Department of Physics and Institute for Pure and Applied Physical Sciences, University of California, San Diego, La Jolla, California 92093

(Received 27 April 1990)

We report muon spin relaxation and rotation measurements on sintered ceramic samples of $Nd_{2-x}Ce_xCuO_{4-y}$ and a large single crystal of Nd_2CuO_{4-y}. We find an electronic phase diagram that is quite similar to that of hole-doped superconductors such as $La_{2-x}Sr_xCuO_{4-y}$, although the doping of electrons into the system is less efficient in destroying the static moments on the copper ions. Static magnetic order appears in Nd_2CuO_{4-y} below about 250 K; two spin reorientations are seen at $T=75$ and 35 K, providing information about the muon site in this material.

I. INTRODUCTION

Since the discovery[1,2] of high-temperature superconductivity in compounds that appear to have electrons rather than holes as charge carriers, there has been considerable interest in the electronic properties of these materials. The mere existence of electron-doped superconductors sheds some light upon certain theories of high-temperature superconductivity. Therefore, to better understand high-T_c systems, it is important to determine the extent to which these new materials are simply negative carrier analogs of the hole-doped systems and the nature of any important differences.

Many studies related to high-T_c superconductors have focused on the changing magnetic properties as the number of charge carriers is varied, converting the materials from antiferromagnetic insulators to metals that eventually exhibit superconductivity.[3] One of the obvious comparisons to make between these systems is whether the electron superconductors have similar electronic phase diagrams. Since the first identification of antiferromagnetism in the undoped parent compounds Ln_2CuO_{4-y} (where Ln represents Pr, Nd, or Sm),[4] we have also studied the electronic phase diagram of $Nd_{2-x}Ce_xCuO_4$.[5] Here we give a comprehensive report of our muon spin relaxation and rotation (μSR) measurements determining the magnetic phase diagram of the $Nd_{2-x}Ce_xCuO_4$ system for $0<x<0.18$. For comparison, we have also studied several specimens of $Pr_{2-x}Ce_xCuO_4$ near the boundary between magnetic order and superconductivity. The resulting phase diagram for these electron-doped materials is compared with that of the analogous hole-doped $La_{2-x}Sr_xCuO_4$ system.

II. MUON SPIN RELAXATION AND ROTATION

The technique of muon spin relaxation[6] has been extensively applied to the study of high-temperature superconductors.[7] Briefly, the positive muon is employed as a pointlike probe of the local magnetic environment around the interstitial site(s) at which it stops. The muon generally occupies a unique crystallographic site, although in complicated crystal structures such as those of the high-temperature superconductors, several sites are sometimes

 ©1990 The American Physical Society

identified.

The muon samples the local magnetic environment through its spin and reveals its polarization through its parity-violating decay (muon lifetime $\tau_\mu = 2.2\ \mu$s), emitting a positron preferentially along the instantaneous spin direction at the time of decay. The numbers of positrons detected in two opposing counters (say F and B, for the forward and backward directions) are given by

$$N_B(t) = N_0^B\{B_B + e^{-t/\tau_\mu}[1 - A_0^B \mathcal{P}(t)]\}\ ,$$
$$N_F(t) = N_0^F\{B_F + e^{-t/\tau_\mu}[1 + A_0^F \mathcal{P}(t)]\}\ , \tag{1}$$

where B_B, B_F correspond to the fraction of time-independent background events, A_0^B, A_0^F are the asymmetries of the B and F counters, and $\mathcal{P}$ is the muon polarization function, These signals have their time-independent background subtracted to give signals $\mathcal{F}(t)$ and $\mathcal{B}(t)$. An experimental asymmetry is then defined:

$$\mathcal{A}(t) = \frac{\mathcal{B}(t) - \mathcal{F}(t)}{\mathcal{B}(t) + \mathcal{F}(t)}\ . \tag{2}$$

This can be inverted to give the corrected asymmetry

$$A_0^B \mathcal{P}(t) = \frac{(\alpha - 1) + (\alpha + 1)\mathcal{A}(t)}{(\alpha\beta + 1) + (\alpha\beta - 1)\mathcal{A}(t)}\ , \tag{3}$$

where

$$\alpha \equiv \frac{N_0^F}{N_0^B} \tag{4}$$

and

$$\beta \equiv \frac{A_0^F}{A_0^B}\ ,$$

which equals $\mathcal{A}(t)$ when $\alpha = \beta = 1$.

Thus, by monitoring the muon decay spectra one can determine the muon polarization function $\mathcal{P}(t)$ which, in turn, reflects the internal magnetic environment of the sample.

There are several different experimental geometries which are useful for μSR experiments. In the transverse field geometry, the muon spins are injected normal to the applied field, and the (generally either two or four) positron detectors are arranged symmetrically around the field. In the longitudinal–zero-field geometry, the muon spins are initially parallel to any applied field, and the positron detectors are arranged forward and backward with respect to the muon polarization on opposite sides of the sample. Initially, surface muons are created with their spins antiparallel to their momenta. The muon spin may be rotated normal to its momentum prior to implantation through the use of a Wien filter (or spin rotator), consisting of crossed electric and magnetic fields. The Wien filter also serves to remove positron contamination from the incoming muon beam. Figure 1 shows the transverse field (spin-rotated) geometry, as well as the zero-longitudinal (both spin-rotated and non-spin-rotated) geometries. The use of the two different zero-field geometries allows one to vary the relative orientation of the initial muon polarization with respect to the sample, without moving the latter. Through the use of spin rotation, it is possible to study the spin evolution of muons which are polarized in the plane of thin samples (which would otherwise not present a large cross-sectional area to the incoming muon beam).

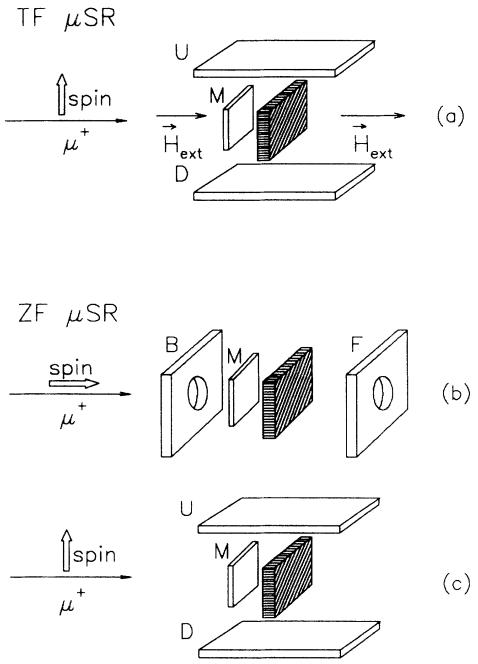

FIG. 1. Experimental geometries for (a) spin-rotated transverse field, (b) non-spin-rotated zero-longitudinal field (ZF-LF), and (c) spin-rotated ZF-LF. Incoming muons detected in the M counter, outgoing positrons detected in the U, D, B, and F counters. The sample is shown as shaded.

In a magnetically ordered material (ferromagnetic or antiferromagnetic), one observes one or more discrete oscillation frequencies in zero applied field, at frequencies given by

$$\omega = \gamma_\mu |\mathbf{B}_{\rm int}|\ , \tag{5}$$

where $\gamma_\mu/2\pi = 13.55$ MHz/kG is the muon gyromagnetic ratio and $\mathbf{B}_{\rm int}$ is the internal magnetic field. It should be noted that the precession frequency is independent of the angle between the local field and the muon spin; only the *amplitude* of the oscillations is reduced when the muon spin is not perpendicular to the applied field. Thus, in a single crystal the magnitude of the oscillating signal can provide information about the directions of the local fields.

The experiments were performed at the M15 and M20B surface muon channels at the TRIUMF cyclotron. These channels provide nearly monochromatic beams of 100% spin-polarized positive muons with momenta of approximately 28 MeV/c. Such muons have a range of about 200 mg/cm^2 which corresponds to a distance of about 0.1 mm in these materials. In the single-crystal studies, the initial muon polarization was prepared either parallel or perpendicular to the crystal $\hat{\mathbf{c}}$ axis using the

Wien filters of M15 or M20B.

The samples were mounted in a He gas flow cryostat, which allowed the temperature to be varied continuously from 3.0 to 300 K. Temperatures were measured using either carbon glass or platinum resistance thermometers.

III. UNDOPED PARENT COMPOUNDS

A. Single crystal Nd_2CuO_4

Zero-field (ZF) μSR measurements on a large single crystal have been used to study both the ordered spin orientations and the muon site in Nd_2CuO_{4-y}. The crystal was grown from a nonstoichiometric CuO-rich solution using a flux method similar to that employed in growing large La_2CuO_{4-y} single cyrstals.[8] The crystal dimensions were $30\times20\times1$ mm^3; the $\hat{c}$ axis was along the thin direction. The sample was mounted with the $\hat{c}$ axis parallel to the incoming beam. The (equivalent) $\hat{a}$ axes were not oriented.

Figure 2 shows ZF μSR spectra at various temperatures below $T_N=252$ K for two different experimental geometries. In Fig. 2(a) the initial muon polarization is along the $\hat{c}$ axis, while Fig. 2(b) is for the case where the initial muon polarization was in the a-b plane. The data at 81 and 25 K are essentially the same for the two different orientations, whereas at $T=55$ K, there is a pronounced difference. In the data taken with the muon polarization along the $\hat{c}$ axis, no precession is seen at 55 K, which indicates that either there is no static internal magnetic field (at the muon site), or the local field is

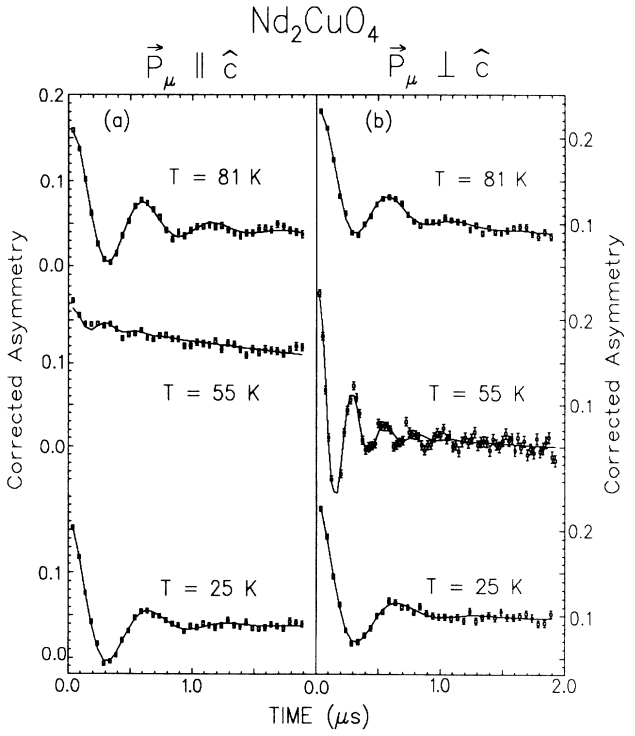

FIG. 2. Zero-field muon spin relaxation for (a) initial muon polarization parallel and (b) perpendicular to $\hat{c}$ axis in single crystal Nd_2CuO_{4-y}.

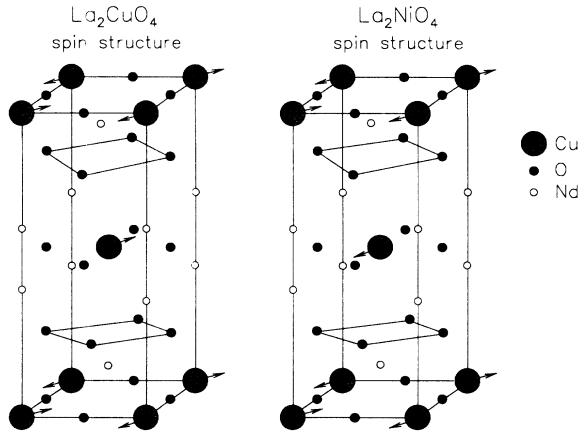

FIG. 3. Crystal and ordered spin structure for Nd_2CuO_{4-y}. Shown in figure are Cu atoms (large shaded circles), O atoms (small solid circles), and Nd atoms (small open circles). In the temperature range $35<T<75$ K, Nd_2CuO_{4-y} orders in the La_2CuO_4 spin structure, otherwise in the La_2NiO_4 structure. Possible muon sites all lie near O atoms in the oxygen planes at $z=0.25$ and 0.75, midway between CuO_2 planes.

directed along the muon spin direction (i.e., along the $\hat{c}$ axis). The observed precession when the initial spin direction lies in the a-b plane [Fig. 2(b)] demonstrates that there is an internal field at the muon site, which is therefore directed along the $\hat{c}$ axis at $T=55$ K (and not at $T=25$ or 81 K).

This spin reorientation has also been observed in neutron-scattering experiments[9] which have shown that the spin structure changes from that of La_2NiO_4 at high temperatures to La_2CuO_4 at intermediate temperatures, reverting to La_2NiO_4 at the lowest temperatures. These two spin structures differ from each other in that the body-centered Cu ion has its spin rotated by 180° as shown in Fig. 3.

The temperature dependence of the muon spin precession frequency below 125 K is shown in Fig. 4. At higher

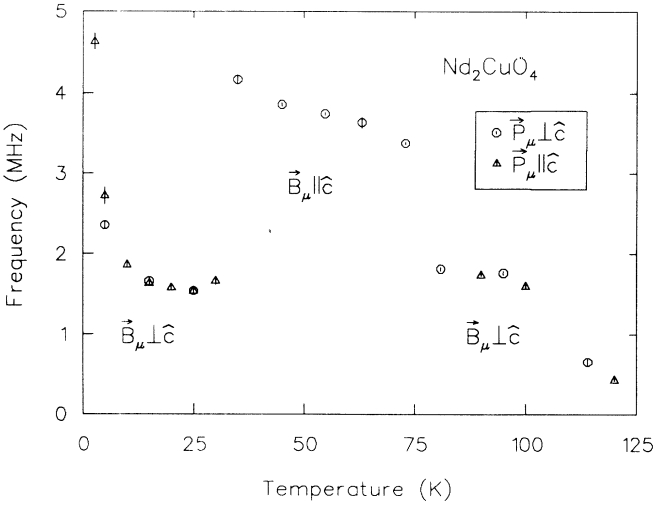

FIG. 4. Zero-field muon precession frequency for muon polarization along the $\hat{c}$ axis and lying in the a-b plane for Nd_2CuO_{4-y}. In the temperature range $35<T<75$ K, precession is observed only for muons polarized in the a-b plane.

temperatures, it is difficult to extract a precession frequency due to the fast relaxation of the signal, though static magnetic fields are clearly visible up to T_N. In the intermediate temperature range $35 < T < 75$ K, precession is seen only for muons polarized in the *a-b* plane. When the muons are polarized along the $\hat{c}$ axis, only longitudinal T_1 relaxation is seen. Figure 4 also shows that the average low-temperature frequency is approximately half as large as the extrapolation to $T=0$ of the frequency in the intermediate temperature phase, the latter being around 6 MHz, about the same as observed in La_2CuO_{4-y}.[10] This difference is a result of the change in the vector sum of the field components from the ordered Cu moments at the muon site between the two different spin structures. We note that the actual frequency abruptly rises at the lowest temperatures, reflecting the onset of ordering of the Nd moments.

We have calculated the local fields throughout the crystal structure for each of the two different spin structures to identify possible muon sites. In these calculations we used the ordered Cu moment of $0.5\mu_B$ determined by neutron scattering[9] and assumed a strictly dipolar field from each copper ion. The criteria for identifying possible sites are that, in the La_2CuO_4 ordered spin structure, the local field must be directed almost entirely along the $\hat{c}$ axis, whereas in the La_2NiO_4 structure, the local field should lie almost exactly in the *a-b* plane. In addition, the field at the muon site should be approximately twice as large for the La_2CuO_4 structure as for the La_2NiO_4 case, as indicated from Fig. 4. The low-temperature frequency corresponding to the La_2CuO_{4-y} structure should be about 6 MHz. Another requirement is that structurally equivalent sites should be essentially magnetically equivalent, since we see only a single magnetically unique muon site.

The candidate sites are all associated with the oxygen plane located at $z=0.25$ (or equivalently $z=0.75$) in the unit cell as shown in Fig. 3. (These are the oxygen ions which correspond to the apical oxygens in La_2CuO_{4-y}.) Most likely, the muon is hydrogen bonded to an oxygen ion in the edge of the unit cell, which lies about 3.5 Å from the nearest Cu ion. The calculated field agrees quite well with the measured muon precession frequencies, showing that the neglect of hyperfine fields on the muon is probably reasonable.

This close association of the muon with oxygen ions has also been seen in muon-nuclear level-crossing experiments with ^{17}O substituted $YBa_2Cu_3O_7$.[11] In addition, ZR μSR measurements[12] have been performed on $Sr_2CuCl_2O_2$ which has the same crystal structure as La_2CuO_{4-y}, with Cl substituted for the apical oxygens. The ZF muon precession frequency [$\nu_\mu(T\rightarrow 0)\sim 16$ MHz] in this material is much higher than in La_2CuO_{4-y} or Nd_2CuO_{4-y}. Furthermore, the orientation dependence of the precession signal amplitude indicates that in $Sr_2CuCl_2O_2$, the local field lies in the plane normal to the $\hat{c}$ axis. Using these two results, comparison of the local fields with calculated field distributions shows that the muon site is in the CuO_2 plane, near an oxygen ion. In the absence of apical oxygen ions (which were replaced by Cl), the muon site changes, with the muon becoming associated with the planar oxygens. There is substantial evidence that the oxygen ions determine the muon site in all of the oxide superconductors via muon-oxygen "hydrogen bonding."[13]

B. Ceramic samples

Sintered ceramic samples were prepared at DuPont and at the University of Tokyo by the usual solid-state reactions as described previously.[1] X-ray diffraction showed that the samples were substantially single phase (μSR is insensitive to small amount, less than a few percent, of impurity phases).

Oscillations of the muon polarization, seen in ZF μSR measurements in the as-grown undoped parent compounds Pr_2CuO_{4-y}, Sm_2CuO_{4-y} (shown in Fig. 5), and Nd_2CuO_{4-y} indicate the presence of static magnetic order. The onset temperature (T_N) for each of these compounds is approximately 250 K. The increased relaxation seen in Sm_2CuO_{4-y} at 5 K is due to the magnetic ordering of the Sm moments, which occurs at 6 K. There was also some increase in the relaxation seen in Nd_2CuO_{4-y} samples at the lowest temperatures studied, presumably due to the slowing down of the Nd moments, which order below 2 K.

In different samples of Nd_2CuO_{4-y}, the ordering temperature was observed to depend on the sample treatment. The onset of order in as-grown (nonreduced) samples was 245 K, whereas in a reduced sample the onset temperature was about 275 K. In comparing the temperature dependence of the magnetic order, much clearer oscillations were observed in the reduced sample at low temperatures and the spin reorientation was clearly visible. In the as-grown material with the reduced Néel temperature, oscillations were not clearly seen; the relaxation was characteristic of much more random magnetic order. For comparison, the single crystal discussed in the preceding section ($T_N=252$ K) shows oscillations intermediate between the two ceramic samples, indicating that its oxygen content was likely between those of the reduced and nonreduced pellets.

The fact that the samples with the higher oxygen content have lower Néel temperatures and have more random order suggests that there is actually a small hole concentration in these samples, frustrating the magnetic order. Reduction is required to remove these holes, first to remove all carriers, improving the magnetic order, then to allow electron superconductivity. Tarascon *et al.*[14] have measured the oxygen concentrations in single crystals of $Nd_{2-x}Ce_xCuO_{4-y}$, and have found that the as-grown crystals have an oxygen content slightly in excess of 4.0, which must be reduced to induce superconductivity.

IV. PHASE DIAGRAM

In determining the magnetic phase diagram, we used a combination of transverse field and zero-field measurements. The application of a weak transverse magnetic field allows one to determine the paramagnetic volume fraction of a sample, since muons, which reside at sites

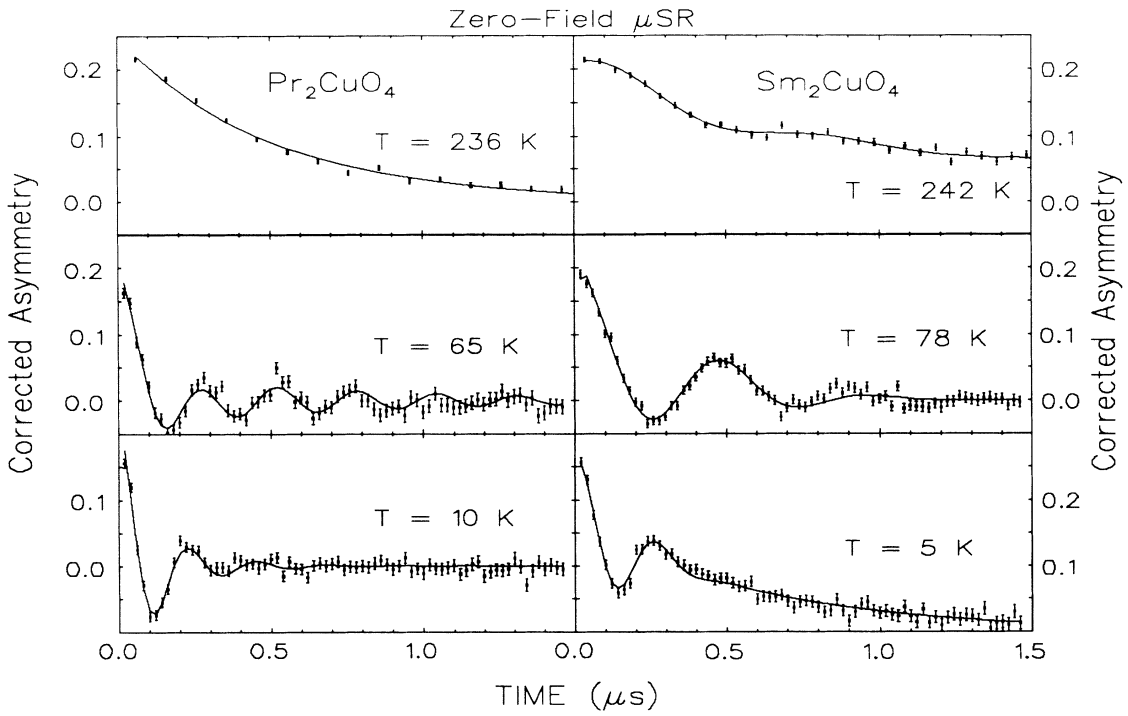

FIG. 5. Zero-field μSR spectra for Pr_2CuO_{4-y} and Sm_2CuO_{4-y} for as-grown (nonreduced) sintered ceramic samples at several temperatures in the ordered state.

with an appreciable magnetic field ($\sim$30 G or greater), are quickly depolarized, whereas others precess coherently in the external field. Zero-field measurements similarly show an increase in the relaxation rate on entering the ordered state. The presence of oscillations in the muon polarization indicates a large degree of uniformity in the local fields throughout the sample, whereas simple relaxation is indicative of a broader distribution of local field strengths in the ordered state.

The effects of doping on these systems was studied through the substitution of Ce for Nd or Pr. The preparation of these reduced samples at the University of California at San Diego, University of Tokyo, and DuPont by solid-state reactions is described in detail elsewhere.[1,16] Typical μSR spectra are shown in Fig. 6 for $Nd_{2-x}Ce_xCuO_{4-y}$ ($x=0.0$, 0.1, 0.14, and 0.16) at $T=10$ K. All of these samples except for the superconducting one ($x=0.16$) exhibit relaxation characteristics of static magnetic order.

Figure 7 shows the ordering temperature as a function of dopant concentration for the $Nd_{2-x}Ce_xCuO_{4-y}$ system. The phase diagram is similar for the (Pr,Ce) system. The first effect of doping is to gradually reduce the Néel temperature from about 250 K for the undoped system ($x=0$) and to increase the apparent randomness in the ordered state. Static order disappears as the dopant concentration approaches that required for superconductivity ($x=0.15$). We note that the boundary region between superconductivity and magnetism is extremely steep

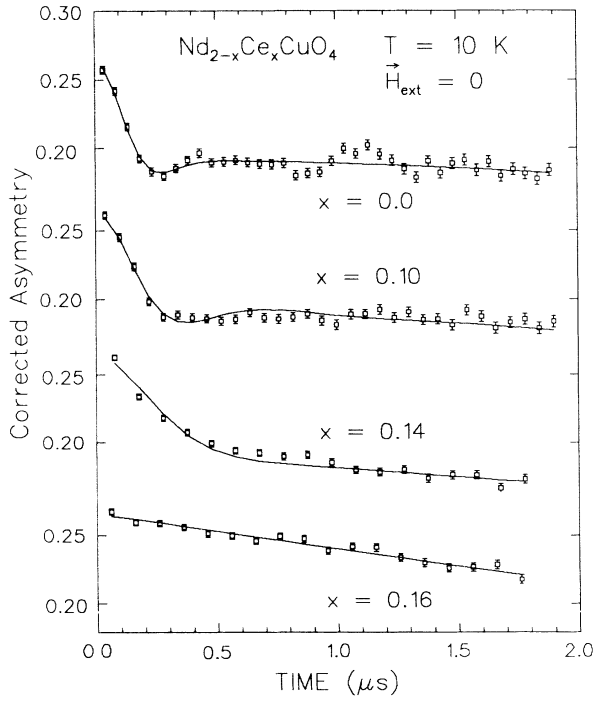

FIG. 6. Zero-field μSR spectra taken at $T=10$ K for $Nd_{2-x}Ce_xCuO_{4-y}$ for $x=0$, 0.10, 0.14, and 0.16.

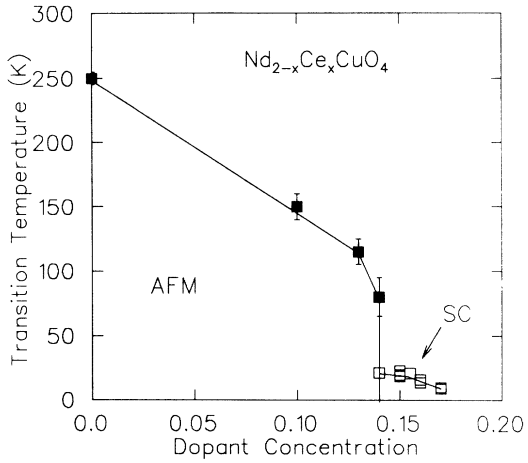

FIG. 7. Electronic phase diagram for reduced $Nd_{2-x}Ce_xCuO_{4-\delta}$ showing antiferromagnetic (AFM) and superconducting (SC) phases. T_c values taken from Ref. 1.

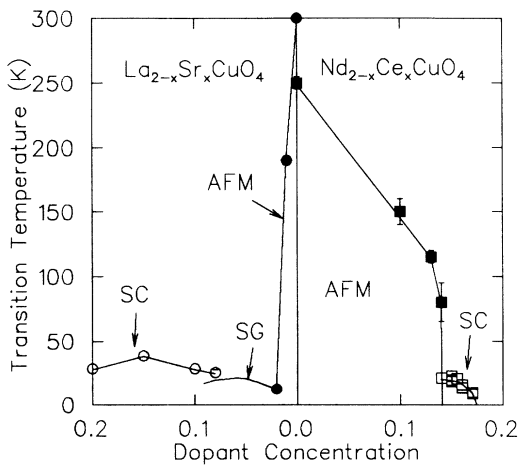

FIG. 8. Electronic phase diagram for both electron (reduced) and hole (oxygenated) superconductors (214-type), showing antiferromagnetic (AFM), spin glass (SG), and superconducting (SC) phases.

around $x=0.15$, dropping from 80 K at $x=0.14$ to below 5 K (i.e., ordering of Cu moments not seen in the temperature range studied) by $x=0.15$. The general effect of doping electrons is similar to that of doping holes in $La_{2-x}Sr_xCuO_{4-y}$, in that it first causes a reduction in the ordering temperature, followed by the destruction of magnetic order at higher doping concentrations. In both systems, superconductivity appears at or near the doping concentration where magnetic order disappears (although this occurs for different x in the two systems).

Electron doping appears far less effective at destroying magnetic order as seen in the $Nd_{2-x}Ce_xCuO_{4-y}$ system, where, even for $x=0.14$, order is seen as high as $T=80$ K. This may be compared to hole-doped $La_{2-x}Sr_xCuO_{4-y}$ where the Néel temperature is reduced to below 10 K for $x=0.02$,[17] with superconductivity appearing around $x=0.075$ (see Fig. 8).

The different effectiveness of carrier concentration for destroying magnetic order in the electron- and hole-doped systems may be understood in two ways. First, the doping of electrons or holes into the system could provide approximately the same number of carriers to the CuO_2 planes, with the differences being ascribed to the different effects of electrons located primarily on Cu ions, and holes, located mainly on the oxygen ions. The doping of electrons changes $Cu^{2+}\rightarrow Cu^{1+}$,[18] filling the copper $3d$ shell and making the copper act like a nonmagnetic Zn ion, effectively diluting the spin system. Hole doping, on the other hand, changes $O^2\rightarrow O^-$. The presence of a magnetic oxygen ion between two adjacent Cu ions serves to provide an effective ferromagnetic interaction between the Cu ions, thus frustrating the antiferromagnetic ordering. The difference in the ability to destroy order is then understood in terms of the greater effectiveness of frustration relative to dilution in destroying magnetic order. Similar results for the varying effects of dilution and frustration have been seen in the $Rb_2(Mn_{1-x}Cr_x)Cl_4$ (Ref. 19) and $Rb_2(Mn_{1-x}Zn_x)Cl_4$ (Ref. 20) systems. The substitution of Mn by (magnetic) Cr quickly frustrates the antiferromagnetic order for x as small as 0.2, whereas, if the Mn is diluted by (nonmagnetic) Zn, antiferromagnetism still exists for x as large as 0.59.

A second possibility is that doping with the same (from a chemical stoichiometric point of view) concentration causes different carrier levels to be actually located on the CuO_2 planes, with the other doped carriers residing elsewhere in the crystal structure. However, this is in disagreement with Hall-effect measurements[21] which show that the Hall coefficient changes quite symmetrically with electron and hole doping. Additionally, it would be difficult to understand why the optimum doping concentration (near $x=0.15$) would be essentially the same for the two different systems if the doped carriers did not go to the CuO_2 planes in an equivalent manner.

The fact that the dopant levels for the *onset* of superconductivity is different for the two systems, even though the *optimal* doping ($x\sim 0.15$) is the same, supports the view that there is a deep connection between the magnetism and superconductivity in these CuO_2 systems. It is clear from these results that, although superconductivity and magnetism occur in close proximity to each other, there tends to be a transition from one state to the other, rather than extensive coexistence. Apparently, the onset of superconductivity is correlated with the destruction of magnetic order, rather than being a separate unrelated phenomenon.

We have also studied a number of nonreduced samples. Figure 9 shows the zero-field muon relaxation in an as-sintered sample of $Nd_{1.845}Ce_{0.155}CuO_4$. Static moments appear around 100 K, much as in reduced samples of $Nd_{1.87}Ce_{0.13}CuO_{4-y}$. When the Ce concentration is increased to $x=0.18$, however, there is little sign of increased relaxation except at the lowest temperatures ($T\sim 10$ K), which is likely due to the slowing down of the Nd moments rather than the presence of static moments on the Cu atoms.

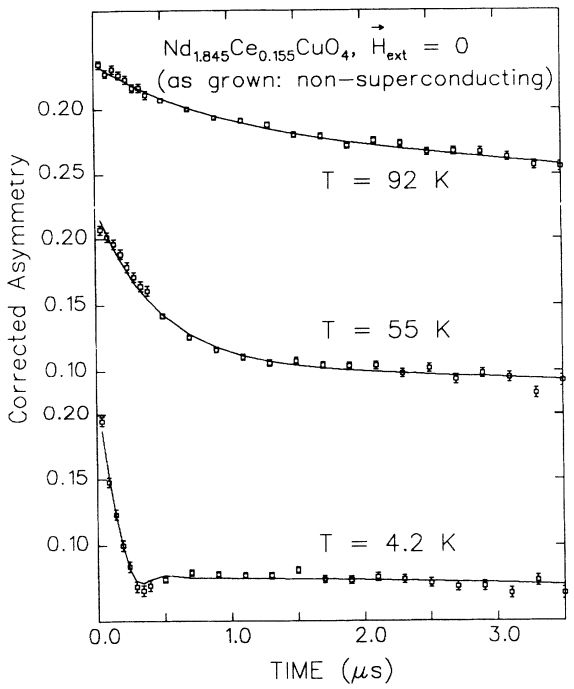

FIG. 9. Zero-field spectra for an as-grown (nonreduced) sample of $Nd_{1.845}Ce_{0.155}CuO_4$ below the ordering temperature.

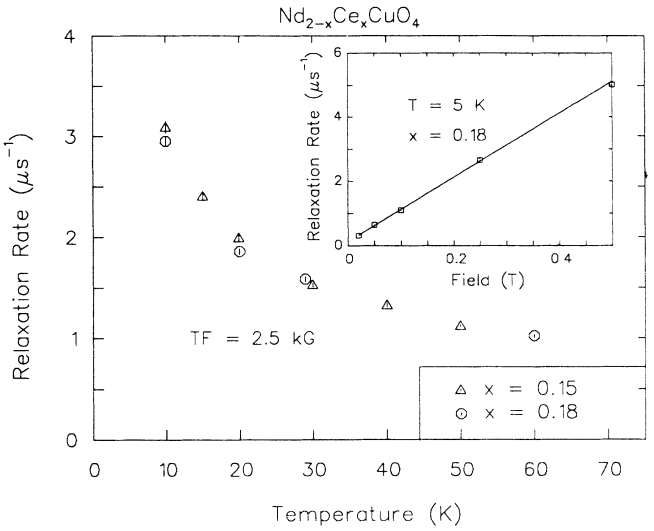

FIG. 10. Transverse field spin relaxation rate for reduced samples of superconducting $Nd_{1.85}Ce_{0.15}CuO_4$ (triangles) and nonsuperconducting $Nd_{1.82}Ce_{0.18}CuO_4$ (circles). Inset: linear field dependence of muon relaxation rate in $Nd_{1.82}Ce_{0.18}CuO_4$ at $T = 10$ K.

V. PENETRATION DEPTH IN ELECTRON-DOPED SYSTEMS

Much of the work done with μSR in high-temperature superconductors has centered on the measurement of magnetic field penetration depths.[22,23] These measurements are made in a high transverse field, where the distribution of local fields in the vortex state of a type-II superconductor causes a depolarization of the muon spins. When the separation of the vortex cores is smaller than the penetration depth λ, the width of the field distribution (and therefore the transverse field relaxation rate) becomes nearly independent of the applied field and inversely proportional to the square of the penetration depth. A large field is also needed to ensure a more uniform flux lattice, using the intervortex repulsion to overcome flux pinning.

Among the interesting results has been the correlation between T_c and the superconducting carrier density divided by the carrier effective mass (n_s/m^*) as revealed through the transverse field muon spin relaxation rate.[22] We have attempted to determine the magnetic field penetration depth λ in electron-doped superconductors by measuring the muon spin relaxation rate in high transverse field (i.e., $B > 1$ kG). We have found, however, that the rare-earth paramagnetism causes a spin relaxation which is much greater than that expected from the field inhomogeneity caused by the formation of a flux lattice. Figure 10 shows the temperature dependence of the muon relaxation rate for reduced samples of superconducting $Nd_{1.85}Ce_{0.15}CuO_4$ and nonsuperconducting $Nd_{1.82}Ce_{0.18}CuO_4$. The relaxation is essentially the same for the two samples and is roughly inversely proportional to temperature, as expected for the rare-earth paramagnetism. Since the observed relaxation rate is proportional to the applied field (shown at $T = 10$ K in the inset of Fig. 10 for $x = 0.18$), the large fields required for the formation of a uniform flux lattice are incompatible with observing the effects of the vortex lattice for penetration depths of the same order as observed in the hole doped superconductors.

We have attempted to observe relaxation due to the formation of a flux lattice in several different systems, including $Nd_{1.85}Th_{0.15}CuO_4$, $Eu_{1.85}Ce_{0.15}CuO_4$, $Pr_{1.85}Ce_{0.15}CuO_4$, and $Pr_{1.85}Th_{0.15}CuO_4$, with similar results. Thus, it seems that some other technique, such as magnetization, will be required to measure the penetration depth λ, or an optical measurement of the plasma frequency to determine n/m^* will be required to test whether the new electron superconductors obey the relation observed in the hole-doped systems.

VI. CONCLUSIONS

The parent compounds Ln_2CuO_{4-y} of the new electron superconductors all exhibit static magnetic order, with Néel temperature around 250 K, just as have all of the parent compounds of the hole-doped CuO_2 superconductors. Nd_2CuO_{4-y} undergoes two additional magnetic transitions involving spin configuration changes at 75 and 35 K, which have allowed us to identify the probable muon site in this material.

As a function of doping, electron-doped superconductors behave in many ways similarly to the older hole-doped CuO_2 planar superconductors in that the CuO_2 planes may be doped with either type of carrier to form a

superconductor. Differences in the details of their respective phase diagrams probably arise from the different effectiveness of the doped carriers in destroying the magnetism of the Cu ions. Apparently, doped holes centered on the oxygen ions frustrate the Cu spin network, whereas electrons are doped onto the copper sites, effectively removing a Cu spin (dilution). Once the magnetism is destroyed, superconductivity occurs. The appearance of superconductivity is tied to the disappearance of magnetism in both the hole-doped and electron-doped systems, underscoring the intimate relationship between magnetism and superconductivity in high-T_c systems.

ACKNOWLEDGMENTS

We would like to thank Dr. V. Emery for useful discussions. Research at Columbia was supported by The National Science Foundation (NSF) Contract No. DMR-89-13784, at University of California at San Diego (UCSD), by U.S. Department of Energy Grant No. DE-FG03-86ER45230, and at Virginia State University by (U.S. Department of Energy Grant No. DE-FG05-88ERA5 353. Research at TRIUMF was supported by the National Sciences and Engineering Research Council (NSERC) and National Research Council of Canada (NRC). One of us (Y.J.U.) was supported by the David and Lucile Packard Foundation.

---

*Present address: Metal Phys. Lab., RIKEN, 2-1 Hirosawa, Wako, Saitama 351-01 Japan.

†Present address: Department of Chemistry, Oregon State University, Corvallis, Oregon 27331.

‡Present address: Department of Physics, University of Texas, Austin, Texas 78712.

[1]Y. Tokura, H. Takagi, and S. Uchida, Nature **337**, 345 (1989).

[2]H. Takagi, S. Uchida, and Y. Tokura, Phys. Rev. Lett. **62**, 1197 (1989).

[3]See, for example, R. J. Birgeneau, and G. Shirane, in *Physical Properties of High Temperature Superconductors I,* edited by D. M. Ginsberg (World Scientific, Singapore, 1989), Chap. 4.

[4]G. M. Luke, B. J. Sternlieb, Y. J. Uemura, J. H. Brewer, R. Kadono, R. F. Kiefl, S. R. Kreitzman, T. M. Riseman, J. Gopalakrishnan, A. W. Sleight, M. A. Subramanian, S. Uchida, H. Takagi, and Y. Tokura, Nature **338**, 49 (1989).

[5]G. M. Luke *et al.,* Physica C **162-164**, 825 (1989).

[6]A. Schenck, *Muon Spin Rotation Spectroscopy: Principles and Applications in Solid State Physics* (Hilger, Bristol, 1985); S. F. J. Cox, J. Phys. C **20**, 3187 (1987).

[7]See, for example, Y. J. Uemura, J. Appl. Phys. **64**, 6087 (1988); Y. J. Uemura *et al.,* Physica C **162-164**, 857 (1989); H. Keller, IBM J. Res. Dev. **22**, 314 (1989).

[8]Y. Hidaka *et al.,* J. Cryst. Growth **85**, 581 (1987).

[9]Y. Endoh, M. Matsuda, K. Yamada, K. Kakurai, Y. Hidaka, G. Shirane, and R. J. Birgeneau, Phys. Rev. B **40**, 7023 (1989); J. Akimitsu, H. Sawa, T. Kobauashi, H. Fujiki, and Y. Yamada, J. Phys. Soc. Jpn. **58**, 2646 (1989).

[10]Y. J. Uemura, W. J. Kossler, X. H. Yu, J. R. Kempton, H. E. Schone, D. Opie, C. E. Stronach, D. C. Johnston, M. S. Alvarez, and D. P. Goshorn, Phys. Rev. Lett. **59**, 1045 (1987).

[11]J. H. Brewer, J. F. Carolan, P. Dosanjh, W. N. Hardy, P. Schleger, R. F. Kiefl, S. R. Kreitzman, Q. Li, T. M. Riseman, H. Zhou, E. J. Ansaldo, L. P. Le, G. M. Luke, Y. J. Uemura, K. Hepburn-Wiley, and C. E. Stronach, Hyperfine Interact., to be published.

[12]L. P. Le, G. M. Luke, B. J. Sternlieb, Y. J. Uemura, J. H. Brewer, T. M. Riseman, D. C. Johnston, and L. L. Miller, Phys. Rev. B **42**, 2182 (1990).

[13]W. K. Dawson *et al.,* J. Appl. Phys. **64**, 5809 (1988).

[14]J. M. Tarascon, E. Wang, L. H. Greene, R. Ramesh, B. Bagley, G. W. Hull, P. F. Miclei, Z. Z. Wang, D. Brawner, and N. P. Ong, Physica C **162-164**, 285 (1989).

[15]W. K. Dawson, R. L. Hutson, R. S. Kow, M. Maez, H. Rempp, M. E. Schillaci, J. L. Smith, J. O. Willis, R. L. Lichti, K.-C. B. Chan, C. Boekema, S. P. Weathersby, J. A. Flint, and J. Oostens, Phys. Rev. B **37**, 9401 (1988).

[16]J. T. Markert, E. A. Early, T. Bjønholm, S. Ghamaty, B. W. Lee, J. J. Neumeier, R. D. Price, C. L. Seaman, and M. B. Maple, Physica C **158**, 178 (1989).

[17]Y. Kitaoka, S. Hiramatsu, K. Ishida, T. Kohara, and K. Asayama, J. Phys. Soc. Jpn. **56**, 3024 (1987).

[18]J. M. Tranquada, S. M. Heald, A. R. Moodenbaugh, F. Liang, and M. Croft, Nature **337**, 737 (1989).

[19]K. Katsumata, J. Tuchendler, Y. J. Uemura, and H. Yoshizawa, Phys. Rev. B **37**, 356 (1988).

[20]R. A. Cowley, G. Shirane, R. J. Birgeneau, and H. J. Guggenheim, Phys. Rev. B **15**, 4292 (1977).

[21]H. Takagi *et al.,* Phys. Rev. B **40**, 2251 (1989); S. Uchida and H. Takagi, Physica C **162-164**, 1677 (1989).

[22]Y. J. Uemura *et al.,* Phys. Rev. Lett. **62**, 2317 (1989).

[23]W. J. Kossler *et al.,* Phys. Rev. B **35**, 7133 (1987); D. R. Harshman *et al., ibid.* **36**, 2386 (1987); F. N. Gygax *et al.,* Europhys. Lett. **4**, 473 (1987); D. W. Cooke *et al.,* Phys. Rev. B **37**, 9401 (1988).